UNIVERSITY OF OKLAHOMA

GRADUATE COLLEGE

HYDROGENATION OF DILUTE NITRIDE MATERIALS FOR AN APPLICATION

TO MULTI-JUNCTION SOLAR CELLS

A THESIS

SUBMITTED TO THE GRADUATE FACULTY

In the partial fulfillment of the requirements for the

Degree of

MASTER OF SCIENCE

By

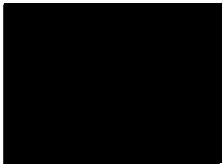MIWA FUKUDA
Norman, Oklahoma
2014

HYDROGENATION OF DILUTE NITRIDE MATERIALS FOR AN APPLICATION
TO MULTI-JUNCTION SOLAR CELLS

A THESIS APPROVED FOR THE
HOMER L. DODGE DEPARTMENT OF PHYSICS AND ASTRONOMY

BY

Acknowledgements

First of all, I would like to appreciate my research and thesis advisor, Dr. Ian Sellers for his aspiring guidance, invaluable constructive criticism and his willingness to motivate me contributed tremendously to the completion of my master's program. He always attended to my questions with patience, grace and humor - even basic questions. I am very fortunate to have such a supportive and friendly advisor whom I owe a tremendous debt of gratitude. Also, I would like to take this opportunity to thank Dr. Vincent Whiteside, a postdoctoral scholar in my research group, whose patience, understanding, attention to details, and assistance made my coursework successful – my deepest appreciation. I also convey endlessly appreciation to my group members – a group of students from varying backgrounds who shared our cultures and chats for fun. I truly enjoyed being part of Sellers' research group and I know those happy moments will last for a lifetime.

Secondly, I wish to express my sincere appreciation to my thesis committee members, Dr. Lloyd Bumm and Dr. Michael Santos. They agreed to be my committee members readily. My thanks to Dr. Mathieu Leroux and Dr. Mohamed Al Khalfioui for providing the samples used in this project and Dr. Khalid Hossain in Amethyst Research Inc. for hydrogenation treatment of those samples. Also my thanks to Dr. Joel Keay and Dr. Matthew Johnson for processing training and letting us use the equipment and cleanroom.

Thirdly, I extend my deepest gratitude to my professors, faculty and friends from Cameron University and University of Oklahoma. I wish to thank my Soka Gakkai International (SGI) family of Oklahoma for their sincere encouragements and support. I am very fortune to have met such wonderful people and have them in my life.

I am eternally grateful to Kobla who encouraged me and helped me ceaselessly with his wisdom and compassion. I wish to avail myself of this opportunity to express a sense of gratitude to my beloved parents and my sister for their moral support, strength, and help for everything, no matter what.

With my best regards and appreciation to all, I would close with a quote from writings of *Nichiren Daishonin*, a Japanese Buddhist. "The journey from *Kamakura* to *Kyoto* takes twelve days. If you travel for eleven but stop with only one day remaining, how can you admire the moon over the capital?" – here, I state my completion of the twelve days journey to admire *the moon* called "*Master's thesis*".

Table of Contents

List of Figures

Abstract

GaInNAs material has been studied as a candidate for the fourth-layer in multi-junction solar cells. However, the material quality of GaInNAs has inhibited its practical use in commercial photovoltaics. While improvements in GaInNAs material using rapid thermal annealing and hydrogenation have been reported, in this thesis, the main focus is on the effects of hydrogenation on GaInNAs solar cells. The selective passivation of impurities/defects and nitrogen-nitrogen clusters by hydrogenation in GaInNAs bulk and solar cell samples is presented. A comparison of reference and hydrogenated solar cells show improvements in the material quality and device performance after passivation.

Chapter 1: Introduction

1.1: Basics and History of Solar Cells

Photovoltaic devices or solar cells are the devices that convert sunlight to electricity. Solar cells have been studied as a clean and abundant form of renewable energy compared to other energy resources such as fossil fuels or nuclear power plants.

The photovoltaic effect was first reported by Edmund Bequerel in 1839 [1][2]. William Adams and Richard Day demonstrated the first solid-state photovoltaic devices forty years later in 1876. They observed that a photocurrent could be produced in a sample of selenium when contacted by two heated platinum contacts. Although solar cells were studied extensively it was not until 1950s when a practical silicon p-n junction solar cell was developed [1]. Daryl Chapin, Calvin Souther Fulter, and Gerald Pearson reported the first silicon solar cell in 1954 at Bell Laboratories. The efficiency was only 6%, which was huge improvement on all previous attempts [1][3]. Other kinds of p-n junction solar cells such as cadmium sulphide or gallium arsenide, indium phosphide, or cadmium telluride were simulated theoretically in the following years. However, it was not until the energy crisis in 1970 that this research accelerated, and solar cells were considered seriously as an alternative energy resource, that the improvement of the efficiency and variety of solar cells produced increased dramatically [1]. Nowadays the highest efficiency solar cells

are the multi-junction solar cells with power conversion efficiencies of more than 40%.

1.2: Solar Cell Material Requirement

To produce high efficiency solar cells, the material needs to absorb light, separate charge carriers, and transport this charge efficiently to generate useable power. In terms of material properties the following are desirable [1]:

(i)   For good optical absorption: high optical depths at energies above the band gap, and small surface reflectivity to improve photon capture.

(ii)   For good charge separation: large built in bias, limited recombination losses, and to locate the junction close to the surface for effective charge separation over a wide range of wavelengths.

(iii) For efficient minority carrier transport: long minority carrier lifetimes and diffusion lengths, and small surface recombination velocities, and low parasitic losses such as small series resistance and high shunt resistance.

(iv)   Optimum band gap close to the intended solar spectrum.

Even if the above conditions are satisfied, there are unavoidable intrinsic losses due to the inability of a single energy gap (E_g) solar cell to correctly match, and therefore harness, the broad solar spectrum. Furthermore, there are also fundamental losses due to radiative recombination [4]. Only photons with $\hbar\omega$ in

excess of E_g are absorbed and generate electron-hole pairs. If the photon has energies lower than E_g it will not be absorbed, but simply be transmitted through the semiconductor. If it has higher energy, the photogenerated electron loses almost all energy in excess of E_g to heat when they relax to energies near the band edges.

1.3: Solar Cell Characteristics and Operation

When measuring or characterizing photovoltaic devices, there are several important terms and electronic properties that arise. The voltage under illumination at zero current is termed the open circuit voltage, V_{OC}. This develops when the terminals are isolated (infinite load resistance). The short circuit current, I_{SC}, is the photogenerated current drawn when the terminals are connected together. The cell develops a voltage V in the range of 0 to V_{OC} and delivers a current I such that $V = IR_L$ where R_L is any intermediate load resistance. The I, V, and R_L are properties of the device and are characterized by the current-voltage response of the solar cell under illumination. Typically, the short circuit current density, J_{SC}, is evaluated rather than I_{SC} because the current is proportional to the illuminated area [1].

(i) Photocurrent Density, Open Circuit Voltage, and Energy:

The photocurrent generated by solar cells under illumination is proportional to the incident light. The photocurrent density is expressed by:

$$J_{SC} = q \int_E^{E+dE} b_s(E) QE(E) dE$$

3

where q is the electronic charge, b_s (E) is the incident spectral photon flux density, and QE is quantum efficiency, which is the probability that an incident photon of energy, E, will deliver one electron to the external circuit.

Energy, E, is defined as:

$$E = \frac{hc}{\lambda}$$

In a more convenient unit for semiconductors, the energy in electron-volt is:

$$E = \frac{1240}{\lambda(nm)} \ (eV)$$

where h is Planck's constant, c is the speed of light in vacuum, and λ is the wavelength of incident photon.

The open circuit voltage, V_{OC}, is the maximum value of potential difference when the contacts are isolated. This is the condition when the saturation current and short circuit photocurrent exactly cancel. It is expressed as:

$$V_{OC} = \frac{kT}{q} \ln \left(\frac{I_{SC}}{J_o} + 1 \right)$$

where k is Boltzmann's constant, T is temperature, J_o is a constant [1].

(ii) *Quantum Efficiency*

Quantum efficiency (QE) is the ratio of the number of charge carriers collected by the solar cell per photon of a given energy incident upon the solar cell. When all photons are absorbed and the resulting minority carriers are collected, the QE at that particular wavelength is unity. For photons with energy below the band gap, the QE is zero. The QE can be considered as the collection probability due the generation profile of a single wavelength integrated over the

4

device thickness and normalized to the incident number of photons. The ideal QE shows the square shape as in Figure 1. However, because of parasitic losses and recombination effects, the practical QE is reduced. The QE takes two forms: external quantum efficiency (EQE), and internal quantum efficiency (IQE). EQE incorporates the effect of the optical losses such as transmission and reflection. That is, it determines the carriers extracted per photon impinging upon the solar cell, which includes the transmission and reflection losses. IQE, however, is the *internal* QE, and considers the current extracted for only for the photons that are absorbed in the cell removing losses associated with reflection and transmission [5].
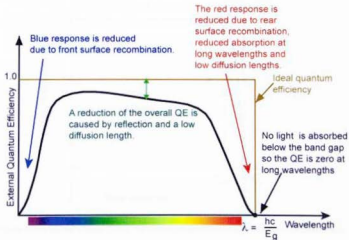
Figure 1: External Quantum Efficiency [5]

Fill factor (FF) is the ideality or 'squareness' of the *J-V* curve and it is defined as

$$FF = \frac{J_m V_m}{J_{sc} V_{oc}}$$

where J_m and V_m are the current density and voltage at the maximum power point (Figure 2).The efficiency, η, is power density delivered at operating point as a fraction of the incident light power density, P_S.

$$\eta = \frac{J_m V_m}{P_S} = \frac{J_{sc} V_{oc} FF}{P_S}$$
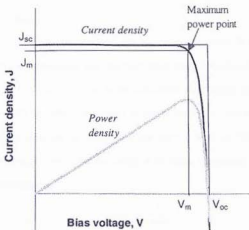
Figure 2: The current voltage (Black) and power-voltage (Grey) characteristics of an ideal cell [1].

Semiconductor devices are temperature dependent. Band gap energy, E_g, of a semiconductor is reduced with increasing temperature due to the thermal expansion of the lattice. This is determined using Varshni's Law given by:

$$E_g(T) = E_g(0) - \frac{\alpha T^2}{T + \beta}$$

where $E_g(0)$, α, and β are dependent on the material [6]. In solar cells, open-circuit voltage is affected by an increase in temperature since the operating voltage is directly proportional to the semiconductor band gap, following the Varshni shift closely.

(i) Air Mass (AM)

Air mass (AM) is conventional unit for solar spectrum. It represents the proportion of atmosphere that the light must pass through before hitting the ground on the Earth relative to its overhead path length [5]. AM 0 is an extraterrestrial spectrum, and AM 1 is when the sun is vertical position. The standard test condition for solar cells is the AM 1.5, which is 1000Wm^{-2} at 25°C. This is corresponding to the sun being at an angle of elevation of 42° [1]. The AM is calculated as

$$AM = \frac{1}{\cos\theta}$$

where θ is the angle of the position of the sun from the vertical [5].

1.4: Single Junction and Multi Junction Solar Cells

The most common solar cell in the market is crystalline silicon solar cell. R.S. Ohl reported the first silicon solar cell, whose efficiency was less than 1% [7][8]. Since this first demonstration, this technology has improved considerably with commercial cells operating with power conversion efficiency (PCE) of ~ 20% on the module. Since silicon technology is a well-developed electronic material, which is abundant and cheap, it dominates the photovoltaic industry. Moreover, the excellent performance of this technology has led to the recent report of a record high efficiency close to 25% for a silicon solar cell [8]. The highest theoretical efficiency, under AM1.5 illumination, predicted for a single band gap semiconductor solar cell is around 30% [4].
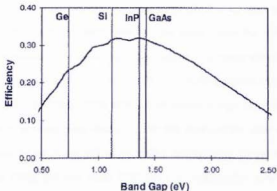
Figure 3: Limiting efficiency as function of band gap for the AM 1.5 solar spectrum, and the band gaps of some common photovoltaic materials [1].

8

Crystalline silicon can absorb radiation greater than 1.12 eV (or below 1100 nm) in solar spectra, which yields a predicted maximum power conversion efficiency of around 27% according to the Shockley-Queisser limit [9], shown in Figure 3. This high efficiency coupled with it is relative low-cost make silicon the current material of choice for PV. However, despite the benefits of silicon, with respect to other materials, the single gap nature of this material limits it overall performance with large regions of the solar irradiation wasted to transmission and thermal losses [10]. To overcome this problem, multi-junction solar cells have been proposed and developed.

Solar cells with two or more semiconducting layers that are stacked as p-n junctions to collect light are called tandem, or multi-junction solar cells. Those layers are assembled with low resistive tunnel junctions and those junctions are formed monolithically on a substrate. The top layer is designed with a higher band gap energy than the layer below it such that higher energy light is absorbed in the upper cells while lower energy, longer wavelength light, is absorbed lower in the stack [11][12]. Through stacking several semiconductor p-n junctions, the multi-junction solar cell can absorb a larger proportion of solar spectra to produce more electricity. The first multi-junction solar cells were introduced by the Research Triangle Institute and by Varian Research Center in the late 1970s and mid 1980s [13][14][11]. In multi-junction solar cells, the current flows serially through the individual cells. Therefore, the current passing through each layer should be matched. If one of the layers produces lower

current, the current produced by the solar cell is limited to the least amount of current. Also, to produce highly efficient solar cells, the system must be of high material quality with each layer lattice matched, or of similar atomic constant. Lattice matching is important because mismatches in the lattice constant lead to defects and dislocations, which form recombination centers that limit performance.

According to a simulation [4], the calculated efficiencies of 1, 2, 3, and 36 serially connected energy gaps are 37, 50, 56, and 72% respectively, at concentration of 1000 suns with the solar cell at 300K. Since the efficiencies of multi-junctions solar cells based on increasingly higher number of layers saturates due to the thermodynamic limit [4], numbers of three to four layers for junctions are the most efficient to stack up.

Chapter 2: Dilute Nitride Solar Cells

2.1: III-N-V Material for Solar cells
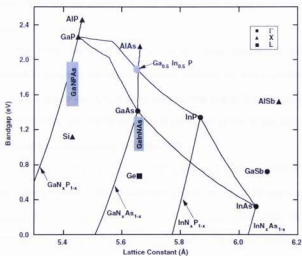
Figure 4: Band gap versus lattice constant. The grey boxes indicate nitrogen-containing alloys that have been grown lattice matched to Ge and Si [15].

The incorporation of a small amount of isoelectronic impurity whose electronic levels are resonant with the host conduction band gap in a semiconductor has been shown as an effective method to engineering the transition energy of several III-V and II-VI semiconductor alloys [16]. The incorporation of small (dilute) amounts of nitrogen into III-V semiconductors has

11

been shown to dramatically change the host band gap. After the discovery of the ability to decrease the band gap energy of GaAs by incorporating nitrogen to form GaNAs by Weyers [17], Kondow et al. demonstrated that the alloy GaInNAs could be lattice matched to GaAs with an absorption energy in the infrared, promoting the potential for the use GaInNAs in long wavelength laser diodes.

The properties of III-N-V material is mainly effected to the large difference in size and the electronegativity between As and N atoms. While nitrogen is isoelectronic, it acts as an electron trap due to this electronegativity difference[18][19]: the crystal potential is deformed at the N site such that a highly localized N-related state is formed [16].

In 1998, Kurtz et al. introduced the idea of the dilute nitride solar cell where it was proposed that GaInNAs with a band gap of 1.0 eV was a potential candidate for the use in 4th layer of multi-junction solar cells [20]. The combination of indium and nitrogen in GaAs could be used in tandem to tune the alloy band gap with increasing indium reducing the energy gap, while increasing nitrogen composition increased the gap [21]. Both lattice matching to GaAs and maintaining a 1eV band gap is required for the optimum efficiency.

In Figure 5, the squares show lattice matching to GaAs with different amounts of In and N incorporation. Here, Vegard's law is assumed for both GaInNAs and GaNAs [22]. Vegard's law is based on a linear relation between the crystal lattice parameter of an alloy and the concentrations of the elements

composing the alloy, at constant temperature [23]. For the lattice matching, the mixing ratio of In and N in alloy $Ga_{1-y}In_yN_xAs_{1-x}$ requires the well known ratio $x:y \sim 1:3$ [22]. This mixing ratio is from $x:y = 0.41:1.14 \sim 1:3$ where those numbers are calculated based on the difference between the lattice constants of GaAs: metastable cubic-GaN (c-GaN) and GaAs:InAs; the difference between GaAs and c-GaN is 1.14 Å and that between InAs and GaAs is 0.41 Å where the lattice constant of GaAs is 5.65Å, c-GaN is 4.51 Å, and InAs is 6.06 Å.
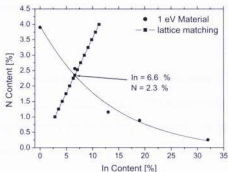
Figure 5: Range of In and N compositions in GaInNAs, for which lattice matching (squares) occurs and for which the samples have a fundamental band gap of 1 eV (circles) [22]

The circles in Figure 5 show the experimental data on a wide range of multiple quantum well (MQW) and bulk samples with different amounts of In and N, which maintain a 1eV band gap. This experimental data is not linear; instead of a linear relationship this behavior is best described by a quadratic one. The parameter for the quadratic term is known as the bowing parameter. For

13

GaInNAs the band gap bowing becomes weaker as the In composition increases. Theoretically, the intersection is where both the requirements are achieved, i.e. lattice matching to GaAs and 1eV band gap for an optimal material [22]. Here, although In=6.6% and N=2.3% are found to be the optimal, other amounts of In and N are used in experiments, such as In=8% and N=2.8%[24], In=9.3% and N=2.1%[25] and In=9% and N=2.8%[26]. The thermodynamic efficiency limit for the III-N-V solar cell – absorbing at 1 eV – incorporated in a 4-junction solar cell grown on germanium is 52%, while for current 3-junction, GaInP/GaAs/Ge systems it is of the order of 40% under AM0 [24][27].

2.2: Problems of Dilute Nitride materials for Solar Cells

Despite its potential GaInNAs as the 4th junction in next generation multi-junction solar cells, there are issues with this material. The synthesis of III-N-V is difficult due to the metastability and large miscibility gap of these materials [28][29][30]. Incorporation of nitrogen into GaAs is not easy. The calculated equilibrium solubility of nitrogen is 0.0000001% at 700°C in GaAs and 0.2% in InAs [31]. However, growing InGaAs at high temperature causes phase segregation [15][32][33]. The bond energy is strongest for Ga-In in GaInNAs so In-As and Ga-N bonds are more energetically favorable and that causes phase segregation and "clusters" of Ga-N and In-As. Nitrogen-related phase segregation must be kinetically limited by growing at low temperature, typically

380-450℃ for molecular beam epitaxy (MBE). These temperature are non-optimum for the Ga(In)As system and incorporate only small fractions of nitrogen. Also, several previous investigations discuss the need for high arsenic fluxes to produce higher quality material. It is suggested that higher group-V fluxes force reactive incorporation of group-III adatoms effectively reducing the surface mobility [34]. Effective growth of this material requires a careful combination of a lower growth temperature limit coupled with an upper limit to the arsenic flux, to inhibit the formation of arsenic anti-sites and other defects that are efficient non-radiative recombination centers [35][36]. Although for 1 eV band gap GaInNAs material, nitrogen incorporation is 2.8%, this composition can lead to significant defect densities and nitrogen cluster formation, which are problematic since such defects decrease the carrier lifetimes and diffusion length of carriers in GaInNAs materials. This leads to reduced voltage and poor quantum efficiencies [28][37][38], reducing the performance of the solar cells.

2.3: Rapid Thermal Annealing (RTA) of GaInNAs

The low growth temperatures required to incorporate nitrogen into GaInNAs to avoid nitrogen-related phase segregation, results in poor material quality; with low – non optimum- temperatures, the growth of Ga(In)As evolves with the formation of various point defects [28]. These defects include group-III vacancies, arsenic anti-sites [36], interstitial nitrogen [39], and even arsenic dimers [40]. All of which degrade the optical quality of the materials. Post-

growth rapid thermal annealing (RTA) has been shown to significantly improve the quality of GaInNAs material [16][24][41]. Although the optimal temperature for RTA is somewhat sample specific, a window of between 800-900°C for 30 seconds has been widely demonstrated.
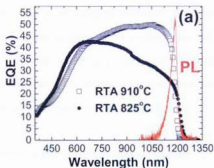
Figure 6: Comparison of external quantum efficiency for GaInNAs solar cells rapid thermal annealed at 825°C (closed circles) and 910°C (open squares). The photoluminescence (PL) for the 910°C device at 300 K is also shown, indicating co-incidence between emission and absorption [41].

Figure 6 [41] shows an example of the improvement of a GaInNAs solar cell after optimized RTA. It shows the external quantum frequency of samples annealed at 825°C (closed circles) and 910°C (open squares) with photoluminescence (PL) of the sample annealed at 910°C. The EQE result of the sample annealed at 825°C shows the well-known sloping behavior at longer wavelengths, which is due to a reduced minority carrier diffusion length in the GaInNAs material at longer wavelengths, between the GaInNAs band gap at

16

1200nm, and the GaAs absorption edge at 870 nm. On the other hand, there is a substantial improvement in performance with a band edge EQE of GaInNAs solar cell annealed at 910°C, both in terms of absolute EQE and minority carrier diffusion length. The more "top-hat" like EQE indicates more efficient carrier collection [41].

The main effect of annealing is considered to be the change of the neighboring configuration of atoms in the crystal lattice [28]. The amount of Ga-N bonds is reduced compared to In-N bonds [42][43]. The improved materials quality reduces the losses to non-radiative recombination and enhances carrier collection and – therefore – EQE [42][44].

2.4: Hydrogenation of III-V and Dilute Nitride Materials

Hydrogen exists in the plasmas, etchants, precursors, and the transport gases of growth processes and device mass production steps [45]. Hydrogen atoms can diffuse into a semiconductor with relative ease and have been used to passivate dangling bonds and defects, resulting in the improved electronic properties of a number semiconductor systems, most prominently in silicon [45][46][47]. The first discovery of the effect of hydrogenation passivation in semiconductors was in ZnO [45]. The effect of hydrogenation has been investigated in several III-V materials [48][49] and recently Polimeni, Capizzi and others reported the result of hydrogenation of GaInNAs [50][45]. In Refs.

[45][50][51], the neutralization of the electronic and optical activity of nitrogen atoms through the formation of N-H bonds was discussed.
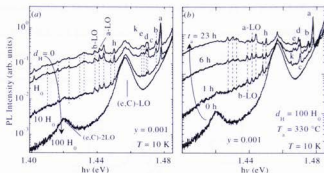
Figure 7: (a) T = 10 K PL spectra of the GaAs$_{0.998}$N$_{0.001}$ epilayer after irradiation at different H dose, d_H. (b) T = 10 K PL spectra of the GaAs$_{0.999}$N$_{0.001}$ epilayer, hydrogenated at d_H = 100H$_0$ for different thermal annealing times t_a (annealing temperature T_a = 330). LO indicates phonon replica transitions, H_0= 5x10^{19} ions cm^{-2} and laser power density P = 10Wcm^{-2} [51].

Figure 7 shows the PL spectra of (a) a hydrogen irradiated dilute nitride sample with different hydrogen doses, and (b) a hydrogenated sample exposed at different annealing times. From Figure 7 (a) increasing the hydrogen dose leads to a progressive and complete quenching of the N-related centers as well as of the broad underlying band. For d_H = 5x10^{15} ions cm^{-2}, only two bands remain, which are related to pure GaAs and the longitudinal optical (LO) phonon replicas of the C-related free-to-bound transition in the GaAs substrate [45]. Such 100% passivation of impurity luminescence bands is extremely unusual and difficult to attain even in the common case of H passivation of shallow

impurities in GaAs or Si [51]. This property is unique to the nitride materials. Figure 7(b) indicates that the hydrogenation effects are fully reversible by thermal annealing. Most of the N-related lines, as well as the broad background beneath them, are progressively recovered by increasing the annealing time. Depending on the strength of the N-H bond, the different lines recover their intensity at different rates [51].
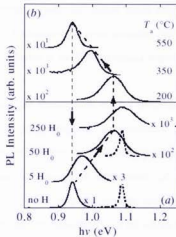
Figure 8: (a) Normalized PL spectra, at 10 K, of the $In_{0.41}Ga_{0.59}As_{0.978}N_{0.022}$ QW for increasing H dose, d_H from bottom to top ($H_0 = 10^{16}$ ions cm^{-2}). Short-dashed lines refer to the $In_{0.41}Ga_{0.59}As$ reference sample. (b) Normalized PL spectra, at 10 K, of the $In_{0.41}Ga_{0.59}As_{0.978}N_{0.022}$ QW with $d_H = 50H_0$ for increasing annealing temperature T_a (1 h duration) and laser power density $P = 102$ Wcm^{-2}. [51]

19

Figure 8 shows the effect of hydrogenation and its reversibility by RTA in GaInNAs. With increasing hydrogen dosage (d_H), the GaInNAs QW band gap blueshifts towards that of the barrier. At the highest d_H, the peak is at the position of the GaInAs band gap. On the other hand, annealing leads to a shift in the band gap back to the original position of the GaInNAs. This behavior suggests Hydrogen can controllably tune the effect of the nitrogen in GaInNAs material. Indeed this has been demonstrated to include the band gap, electron effective mass, exciton wavefunction extent, lattice constant, and temperature coefficient [45][51]. Furthermore, thermal annealing can provide the activation energy to break the bonds of the N-H complexes responsible for these effects [45].

In this thesis, an investigation for the potential for improvements in GaInNAs solar cell performance will be presented. Specifically, the work described investigated the potential to selectively passivate nitrogen clusters and defects known to reduce the performance of GaInNAs solar cells. Improvements of the material quality through hydrogen passivation of the nitrogen-nitrogen clusters and defects in solar cell will be discussed.

Chapter 3: Experimental Procedure and Setup

3.1: Sample Descriptions

In this project, a combination of GaInNAs bulk reference samples and solar cell devices were investigated. The GaInNAs samples were grown using solid-source molecular beam epitaxy (MBE) on n-type GaAs substrates at CRHEA-CNRS in France. Nitrogen radicals were generated from high-purity (6N5) N_2 gas using a radio frequency plasma source (ADDON). For n- and p-type dopants, Si and Be were used, respectively. The GaAs was grown at 580°C and $Ga_{0.91}In_{0.09}N_{0.028}As_{0.972}$ was grown at 450°C.

Figure 9: The structure of bulk sample S1098 (left), I = 500 nm solar cell sample S1095 (middle), and I = 1 μm solar cell sample S677 (right).

#S1098 – Reference Bulk Sample

The GaInNAs bulk sample has a 1.0 μm $Ga_{0.91}In_{0.09}N_{0.028}As_{0.972}$ layer terminated with a 75 nm GaAs cap layer for optical measurements (Figure 9 left). The samples were post-growth annealed in nitrogen-rich conditions at 800°C for 30s. Thermo-power measurements revealed that the nominally intrinsic GaInNAs samples used in the project are slightly n-type in nature due to the non-ideality of the growth conditions [52]. For the hydrogenated sample of S1098, a UV-activated hydrogenation process was developed at Amethyst Research Inc. The combination of low temperature and UV-activation is beneficial in that it reduces the impact damage typically observed in conventional high-energy irradiation processes commonly used for hydrogenation [26][53]. To determine the concentration of hydrogen, deuterium (instead of protium) is used to distinguish it from environmental hydrogen; concentration analysis was performed using nuclear reaction analysis. The sample S1098 was determined to have an optimized hydrogen concentration of 1.1×10^{15} cm^{-2} that has a penetration depth of approximately 2 μm.

#S1095 – Lower quality solar cell sample

The GaInNAs solar cell sample #S1095 was grown in a series of devices used by the MBE growers to evaluate the effects of the intrinsic layer thickness. This sample (Figure 9 middle) consisted of the following structure: The lower base region of the device consists of a 200 nm n-type (6×10^{18} cm^{-3}) buffer layer, then followed by 350 nm of n-type GaAs doped at 1×10^{18} cm^{-3}; the intrinsic region is

a 500 nm layer of nominally intrinsic $Ga_{0.91}In_{0.09}N_{0.028}As_{0.972}$ grown at 450°C; the emitter region has two layers: a 250 nm p-doped ($1x10^{18}$ cm^{-3}) GaAs layer with a 30 nm $Al_{0.7}Ga_{0.3}As$ window layer with the same doping concentration; the structure is finally completed with the deposition of a highly p-doped ($5x10^{18}$ cm^{-3}) 250 nm GaAs contact layer. The post-growth rapid thermal annealing was conducted at 800°C for 30 seconds. In addition to this reference sample, two hydrogenated samples were prepared using the same sample, taken from the original via cleaving. Hydrogen irradiation was performed at Amethyst Research Inc. as described previously for #S1098. The two hydrogenated samples were passivated with hydrogen levels of $1.0x10^{14}$ cm^{-2} (low concentration) and $1.0x10^{15}$ cm^{-2} (high concentration).

#S677 – Higher quality solar cell sample

The GaInNAs solar cell sample #S677 (Figure 9 right) was grown in a series of devices used by the MBE growers to evaluate the potential of doped GaInNAs in these devices. This is an advanced structure in use for solar cells. This sample consisted of the following structure: The lower base region of the device consists of a 0.5 μm n-type buffer layer doped to $4x10^{18}$ cm^{-3}, followed by 0.3 μm of n-type $Al_{0.7}Ga_{0.3}As$ for a back surface field (electronic confinement) layer and 0.2 μm of n-type ($5x10^{17}$ cm^{-3}) GaAs. The intrinsic region consists of an n- and p- type doped GaInNAs – 0.1 μm n- type GaInNAs doped $1x10^{17}$ cm^{-3}, 1 μm thick nominally intrinsic GaInNAs, and 0.1 μm p-type GaInNAs doped $4x10^{18}$ cm^{-3} grown at 400°C. The active region was followed by the emitter

region that consists of a 0.5 μm p-doped GaAs layer and a 0.05 μm $Al_{0.8}Ga_{0.2}As$ window layer doped to the same level. This structure was completed with the deposition of a highly p-doped GaAs contact layer (Figure 9). Post-growth annealing was conducted at 825°C for 30 seconds. In addition to this reference sample, one hydrogenated sample was prepared using the same material, taken from the original via cleaving. Hydrogen irradiation was performed at Amethyst Research Inc. as described previously for #S1098. The hydrogenated sample was passivated with a hydrogen density of 8.7×10^{14} cm^{-2}.

3.2: Device Fabrication Procedure

All dilute nitride solar cell samples were processed into devices using standard semiconductor device fabrication techniques. All processing for this project was performed in the Nielson Hall cleanroom at OU by the author. A detailed description of this process follows:

Samples are cleaved in the size needed. Typical device geometries fabricated in this project ranged from 1 mm^2 to 25 mm^2. For the solar cell, #S677 (l = 1μm), the devices were fabricated using the 2.5 mm x 2.5 mm (6.25 mm^2) solar cell design.

Cleaning; the cleaved samples were cleaned in an ultrasonic bath via a triple solvent process to remove residual dirt and dust particles from the sample surface. The triple solvent process consisted of a 5-minute sonic bath of trichloroethylene (TCE), acetone, and isopropanol (IPA) in succession. After

cleaning the samples the main processing steps were performed. These are listed below:

RTA: Dilute nitride samples are annealed after the cleaning to improve the material quality. For #S677, the annealing temperature was 825°C for 30 seconds in a custom-built AG Associates Heatpulse 610 annealer.

Oxide Removal: To create a uniform surface and improve adhesion of the contact during metallization a chemical oxide removal is applied. The etchant used to remove the residual oxide is a mixture of NH_4OH: DI H_2O in 1:20 ratio, in which the samples are immersed for 30 seconds. After etching, the samples are rinsed by DI water for 1 minute.

Upper electron metallization/photolithography (Negative): To remove any residual moisture, the samples are then baked at 150°C for 10 minutes. Photoresist is then applied to the sample and spun at 4000 revolutions per minute (rpm) for 40 seconds. This is followed by a soft bake for 60 seconds at 95°C on a hot plate. The photoresist is then exposed with UV radiation for 2.5 seconds with a standard 275 W Xenon bulb illuminated via a mask used to define the upper finger electrodes using a Susse-MJB3 mask aligner. The sample is then "soft-baked" on hot plate for 90 seconds at 120°C. This is followed by a flood exposure under UV radiation for 50 seconds without the mask. Here, the previously unexposed area loses its photosensitivity and becomes soluble in the developer solution. The unwanted photoresist is then

removed ("developed") in AZ 1:1 developer for 60 seconds. The sample is then rinsed with DI water for 2 minutes and dried with N_2 gas.

Plasma Ash: A "descum" process was then performed on the sample using an oxygen plasma to clean the sample and remove any residual photoresist. The conditions were set at 55 W for 5 minutes using a March Plasmod GCM 200 system. A hard bake was then carried out on hot plate for 1 minute at 120 °C to harden the resist pattern for durability.

Evaporate Finger Contact: Metallization of the top ohmic p-contact for the device proceeded via the thermal deposition of 5 nm Au, 20 nm Zn, and 250 nm Au.

Finger Liftoff: The pattern of the finger electrodes was exposed using 1165-Strip remover to "lift-off" the unwanted metal. The samples are soaked for 5 to 10 minutes to enable this process, agitating by hand – if required – to promote removal. The sample is then rinsed with DI water.

Cleaning: Agitate samples by hand in acetone and IPA for 5 minutes each.

Contact RTA: To promote adhesion, contact anneal at 420°C for 30 seconds.

Mesa Photolithography (Positive): Prior to mesa etch, the samples are baked at 150°C for 10 minutes to remove any remaining moisture. Photoresist is then applied to the sample and spun at 4000 rpm for 40 seconds. This is followed by a soft bake for 60 seconds at 95°C. The sample is then exposed under the mask aligner according to a second mask to define the mesa profile. This is

then "developed" for 60 seconds. The sample is then rinsed with DI water for 2 minutes, and dried with N_2 gas.

Plasma Ash: The sample is then cleaned using the oxide plasma, removing residual photoresist that is not removed during development. The conditions for this process were once again 55 W for 5 minutes. The sample was then hard baked on hot plate for 1 minute at 120°C.

Mesa Etch: The etchant used to produce the mesa diode is a 2:1:20 mixture of HN_4OH: H_2O_2: DI H_2O. The etching time is varied depending upon the sample conditions and materials. For sample #S677, this required an etching time on the order of 4-7 minutes. To ensure the correct mesa etch depth, each sample is measured using an Ambios-XP2 profilometer. Thereafter, the photoresist is removed in acetone.

Finger/Window Etch: The final wet-etching step is used to remove the contact layer between the finger contacts using a 1:2:200 mixture of HN_4OH: H_2O_2: DI H_2O. The etching time is, again, variable with the sample conditions and materials. For #S677, about 13-30 seconds etching time is needed to remove the cap layer.

Back Contact Deposition: The lower "back" p-type ohmic contact is an alloy of InGe-Au which is thermally evaporated in the following sequence: 20 nm In-Ge, and 200 nm Au.

Contact RTA: The device was then annealed to improve metal adhesion and diffusion the metals into the device to produce high-quality ohmic contacts. The specific conditions for this anneal were 420°C for 30 seconds.

Taking pictures: After each step, pictures of the device are taken to observe the surface using an optical microscope (Figure 10).
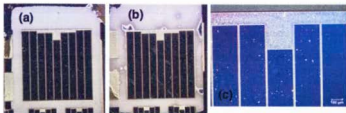
Figure 10: (a) #S677 hydrogenated sample, (b) #S677 reference sample, and (c) magnified #S677 hydrogenated sample.

3.3: Experimental setup

Photoluminescence (PL)

Temperature dependent PL was measured in a Janis closed-cycle cryostat between 4.2 K and 300 K using HeNe laser excitation at 632.8 nm, dispersed with a Princeton instruments 2560i spectrometer, and detected using a liquid nitrogen-cooled InGaAs linear array. A HeNe laser is focused by a 25 mm lens (f = 200 mm) on the samples. The emission is collected by a 2 inch (50 mm) collimating lens (f = 100 mm) and a 50 mm focus lens (f = 250 mm). There is a
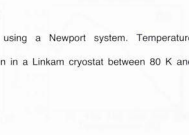
715 nm long-pass filter in front of the focus lens to block the laser line from entering the spectrometer.

Current and voltage (I-V) characteristic

Solar cell I-V analysis was performed using a Newport Class ABA solar simulator under 1-sun conditions. Temperature dependent I-V characteristics were taken in a Linkam THMS600E cryostat between 80 K and 320 K.

External Quantum Efficiency (EQE)

Solar cell EQE was measured using a Newport system. Temperature dependent EQE spectra were taken in a Linkam cryostat between 80 K and 320 K.

Chapter 4: Results and Discussions

4.1: Optical Observations of Hydrogen Irradiation Effect to GaInNAs Material - #S1098 Reference Bulk Sample
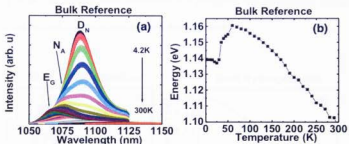
Figure 11: Reference bulk GaInNAs sample (#S1098). (a) Temperature dependent PL, 4.2 K (upper) to 300 K (lower). (b) The peak energy position for each temperature of (a).

Figure 11(a) shows the temperature dependence of the PL for the reference GaInNAs bulk sample. At low temperature, the peaks that are attributed to the lower energy nitrogen clusters (N_A) and defect centers (D_N) are dominant. With increasing the temperature, a transition in the peak PL from that associated with defects (D_N) to that attributed to localized nitrogen-related isoelectronic centers (N_A) is observed. As there is further increase in temperature, the PL finally transitions to that dominated by free excitonic transition. These transitions are reflected by the "s-shaped" dependence of the peak PL energy versus temperature shown in Figure 11b. This is a common

characteristic in dilute nitride materials, which it is due an electronegativity difference caused by the substitution of nitrogen with arsenic. That is, since the electronegativity in N is much larger than As, electrons are more localized around the nitrogen atoms, and therefore positive holes are attracted by Coulomb force, creating an excitonic complex. When the temperature is low (T < 30 - 40 K) this effect dominates, but increasing the temperature causes those carriers to redistribute to higher energy states.

Figure 12: Hydrogenated bulk GaInNAs sample (#S1098). (a) Temperature dependence PL, 4.2 K (upper) to 300 K (lower). (b) The peak energy position for each temperature of (a).

Figure 12 shows: (a) the temperature dependent PL and (b) peak energy of the bulk GaInNAs sample after hydrogen irradiation. The effect of hydrogen passivation is evident in the improvement in material quality for this sample; as seen by the removal of the luminescence from the low-energy defect centers, and a spectral narrowing of the dominant PL emission. The passivated sample

shows the classical Varshni behavior in the peak energy (Figure 12b), which is attributed to band-to-band or free-excitonic luminescence. Previous reports [51][45] of hydrogenation of GaInNAs have also observed the passivation of nitrogen centers and defect-related transitions using PL. However, in those reports, the *complete removal of the effect of nitrogen from the alloy* was observed *before* any evidence of the removal of the "s-shape" behavior was demonstrated (See Chapter 2) [51]. This occurred because of the complete passivation of N in the alloy to form N-H bonds in these previous works. This resulted in a blueshift in the band gap energy to that of the host materials. In this thesis, the complete removal of substitutional nitrogen is avoided as seen in the PL position, which is attributed to the free excitonic transitions, once the passivation of N-N clusters or defects is optimized. This suggests that the hydrogen passivates the N-N clusters or defects prior to passivating the N in the alloy.

Since hydrogen passivates both donors and acceptors, including vacant isoelectronic centers in GaInNAs [54], the elimination of the localized isoelectronic emission at low temperature observed in Figure 12b is considered to be the result of hydrogen passivation of donor impurities [52]. Previous studies of our materials [52] indicated that the background impurity concentration is n-type and that these donor electrons are localized in N-cluster and acceptor levels. This results in intense emission, through recombination of photoexcited holes and localized donors in PL measurements. However, a

slight p-type co-doping of the materials was observed to passivate donors bound to the nitrogen isoelectronic centers; removing the effects of localized recombination due to the dominance of faster – more efficient – band-to-band recombination [52].

4.2: Optical Observations of Hydrogenation Effect to GaInNAs Solar Cell Material - #S1095 Low quality solar cell

The effect of hydrogen passivation was also examined in GaInNAs solar cell material. The structure of these devices is a p-i-n diode, which was introduced in Chapter 3 (Figure 9).

4.2K I=500nm Reference
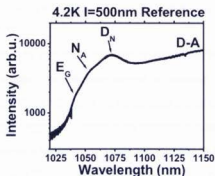
Figure 13: 4.2 K PL of reference solar cell (#S1095). The axis of intensity is in logarithm scale.

Figure 13 shows the PL at 4.2 K of the reference solar cell sample. In GaInNAs materials, in addition to the D_N states, there is a large impurity band due to donor-acceptor (D-A) transitions at > 1125 nm, which is not shown fully

in the temperature dependent results for clarity. This is attributed to p- and n-type dopants in the GaAs regions of the solar cell structure.
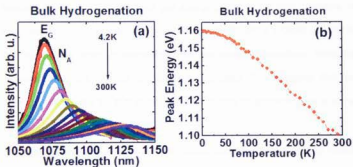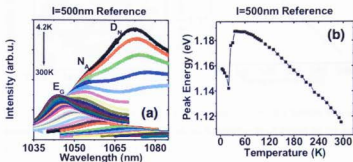

Figure 14: Reference -RTA 800°C non-hydrogenated GaInNAs solar cell sample (#S1095). (a) Temperature dependent PL, 4.2 K (upper) to 300 K (lower). (b) The peak energy position for each temperature of (a).

Figure 14a shows the temperature dependent PL of the reference GaInNAs sample. The reference sample is annealed at 800°C and not hydrogenated. Figure 14b shows the highest peak energy extracted from the PL measurement in Figure 14a. Similar to the reference bulk sample, this reference solar cell sample is dominated by a large impurity band (D_N) around 1075 nm at low temperatures (Figure 14a). The peak energy again – therefore – shows the "s-shape" transition (Figure 14b) as observed in the bulk reference material.
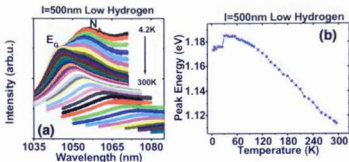
Figure 15: RTA 800 °C and UV-hydrogenated in low hydrogen concentration GaInNAs solar cell sample (#S1095). (a) Temperature dependent PL, 4.2 K (upper) to 300 K (lower). (b) The peak energy position for each temperature of (a).

Figure 15a and 15b show the same solar cell structure (material) with a hydrogenation concentration of 1.0×10^{14} cm^{-2}. Again, as seen in the hydrogenated bulk sample, the peaks due to the defects or impurities are dramatically quenched. In the solar cell material with this relatively low concentration of hydrogen, the peaks related to the isoelectronic centers (N_A) are dominant at low temperatures, until thermal delocalization (T > 30 K) enables a transition to the dominance of band-to-band peaks (Figure 12a).
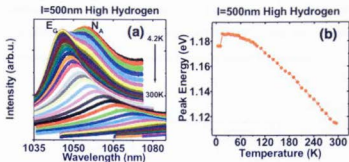
Figure 16: RTA 800 °C and UV-hydrogenated in high hydrogen concentration GaInNAs solar cell sample (#S1095). (a) Temperature dependent PL, 4.2 K (upper) to 300 K (lower). (b) The peak energy position for each temperature of (a).

Figure 16a and 16b show the same material with a *higher* hydrogenation concentration of 1.0×10^{15} cm^{-2}. Again, it is observed that the passivation process reduces the effects of defects and impurities. Though the higher hydrogen concentration is "high" relative to the lower hydrogenation process, the higher hydrogen concentration is too low to totally eliminate the contribution of all the centers. This is due to the large concentration of defects and impurities in solar cell material compared to the bulk sample, which is expected in a thicker and more complicated structure.

Comparing the hydrogenation effect in the reference, low concentration, and high concentration, it is clear that clusters and/or larger defects and impurities, D_N, that dominate the PL in the reference solar cell material (Figure 14a) are passivated. The PL evolves from that of delocalized transitions, N_A, to

36

eventually band-to-band recombination, E_G, when the samples are hydrogenated (Figure 15a and 16a). This indicates that the selective passivation of defects and impurities is translated to solar cell devices.
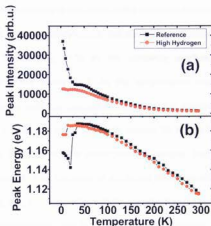
Figure 17: (a) Comparison of PL highest intensities of the reference solar cell sample (#S1095) (black squares) and the highest hydrogen concentration irradiated solar cell sample (#S1095) (red circles). (b) Comparison of peak energies of the reference solar cell sample (#S1095) (black squares) and the highest hydrogen concentration irradiated solar cell sample (#S1095) (red circles).

Figure 17 is the comparisons of the PL of the reference and hydrogenated GaInNAs solar cell samples. Figure 17a, shows the PL peak intensities of the reference sample (black circles) and a hydrogen irradiated sample (red squares) extracted from the temperature dependent PL. In Figure

17b, a comparison of the peak energies of the reference and hydrogenated devices is shown. In Figure 17b, a significant drop in intensity for the reference sample is seen with increasing temperature in the range of T < 30 K. Thereafter, the intensity stabilizes until 50 K, when it decreases further with increasing temperature. This behavior is attributed to the localized nature of the carriers. In the area where the intensity drops, the carriers are thermally activated from lower energy levels (D_N, D-A) to the relatively shallow, higher energy, isoelectronic acceptor levels (N_A). As the temperature increases, the peak intensities saturate until the carriers localized in the shallow acceptor levels reach thermal equilibrium with the bands around 50 K. On the other hand, at T < 50 K the intensity of the hydrogenated sample (red circles) remains relatively consistent. This behavior is attributed the removal of the effects of localized states, and the passivation of donors bound to isoelectronic centers.

For all temperatures, the PL intensity of the reference sample is brighter than that of the hydrogenated samples. It is considered that this is related to an improved carrier mobility, which serves to decrease recombination pathways potentially increasing carrier extraction in photovoltaic devices. This observation is discussed in the next section using the processed solar cell devices.

4.3: Electronic Observations of Hydrogenation of GaInNAs Solar Cell Material - #S677 High Quality Solar Cell

In previous our work, the reference and hydrogenated samples of #S1095 were processed and analyzed [26]. However, the material was non-optimum in terms of quality. Therefore, the reproducibility during device fabrication was poor, which was attributed to alloy fluctuations and inhomogeneities across the wafer. As such, any comparison of device performance was unreliable. The sample #S677, however, is of higher quality than previous structures, with relatively homogeneous material quality in comparison to #S1095.
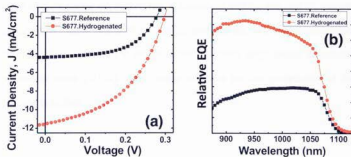
Figure 18: (a) Current density - voltage (J-V) measurements of 2.5 mm x 2.5 mm devices of reference (black squares) and hydrogenated (red circles) material from #S677. (b) EQE measurements of 2.5 mm x 2.5 mm devices of reference (black squares) and hydrogenated (red circles) material from #S677.

To compare the device performance, all the various #S677 samples were fabricated into 2.5 mm by 2.5 mm (6.25 mm²) solar cells during the same processing run for consistency and to limit anomalies.

Figure 18 shows the (a) current density-voltage characteristic and (b) EQE spectra of the reference (black squares) and hydrogenated (red circles) solar cells. The total hydrogen concentration was determined to be 8.7×10^{14} cm^{-2}. In Figure 18a, the Jsc and Voc of the hydrogenated sample is improved relative to the reference. The Jsc of the hydrogenated sample is about three times that of the reference. This is also reflected in a significant improvement in the EQE of the hydrogenated sample with respect to the unpassivated cell as seen in Figure 18b. The large improvement in EQE (and Jsc) reflects lower losses and more efficient carrier extraction. This is consistent with the reduced PL intensity observed in Figure 17b for the hydrogenated sample. Previous investigations have indicated that even in higher quality GaInNAs large losses to radiative processes occur [41][42]. Here, some evidence for the perturbation of this process is evident.
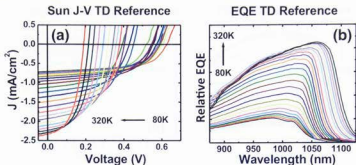
Figure 19: (a) Temperature dependent current density - voltage characteristics with temperatures from 80 K (right) to 320 K (left) and (b) temperature dependent EQE with temperatures from 80 K (lower) to 320 K (upper) of reference higher quality solar cell material (#S677).

Figure 19 shows the (a) temperature dependent J-V and (b) temperature dependent EQE of the reference sample #S677. In Figure 19a, there are fluctuations in Voc at lower temperatures. Figure 19b shows an increasing EQE as the temperature increase, which indicates enhanced thermally activated carrier extraction and the existence of localized centers. The energy dependent shift of the absorption edge can be somewhat accounted for by the thermal expansion of the lattice at increasing temperatures, although the large increase in EQE suggests further, as yet unknown, processes also play a role.
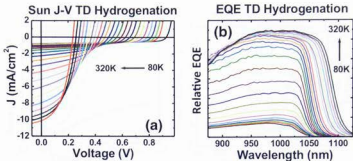
Figure 20: (a) Temperature dependent current density - voltage characteristics with temperatures from 80 K (right) to 320 K (left) and (b) temperature dependent EQE with temperatures from 80 K (lower) to 320 K (upper) of hydrogenated higher quality solar cell material (#S677).

Figure 20 shows (a) the temperature dependent J-V from 80 K to 320 K and (b) the temperature dependent EQE from 80 K to 320 K for the hydrogenated sample. As compared to the reference (Figure 19), the relative change in J-V with temperature is more uniform, while the EQE has a more "top-hat" shaped response indicative of improved minority carrier lifetime. The increased carrier extraction observed for the hydrogenated solar cell may also reflect a reduced background impurity concentration, which would increase the depletion width across the intrinsic region of the p-i-n structure. Capacitance-Voltage measurements are planned to evaluate this property.
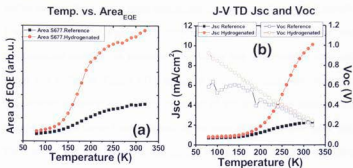
Figure 21: (a) The area of EQE extracted from temperature dependent EQE of the reference sample (black filled square) and the hydrogenated sample (red filled circle). (b) Short circuit current density of the reference sample (black filled square) and the hydrogenated sample (red filled circle), and open circuit voltage of the reference sample (black open square) and the hydrogenated sample (red open circles) extracted from temperature dependent *J-V* measurements.

Figure 21a shows a comparison of the integrated EQE for the GaInNAs absorbing region (between 870 nm and 1200 nm) at each temperature for the reference (black filled square) and the hydrogenated solar cells (red filled circle). The integrated EQE is directly related to the current density produced by the solar cell device as shown in section 1.3 in Chapter 1. The gap between the areas of the hydrogenated sample and reference sample is dramatically spaced out. This implies that the hydrogenated sample produces more photocurrent. Figure 21b shows the *Jsc* and *Voc* for each temperature. The black filled squares represent the *Jsc* and black open squares, the *Voc* of the reference sample extracted from temperature dependent *J-V* characteristics. The red filled

circles are the Jsc and red open circles, the Voc of the hydrogenated sample. The Jsc behavior in Figure 21b reflects the behaviors of reference and hydrogenated samples, as expected. The Voc of the hydrogenated solar cell (open red circles in Figure 21b) shows a linear decrease with increasing temperature, following the thermal reduction of the energy gap although the change in Voc is larger than expected. In the case of the reference solar cell, the Voc fluctuates at lower temperatures, indicating an effect of operating voltage limited by localized centers and thermally activated carrier processes. The large difference in Voc at lower temperatures between the two solar cells, with the hydrogenated sample almost 0.5 V larger, indicates, again, the reduction of non-radiative centers at lower temperatures. As the temperature increases, however, the Voc between the two samples becomes comparable with similar Voc values observed at T > 200 K. This large change in the Voc, which is also reflected in the large – non incremental - transition in the illuminated Jsc versus Voc curves (Figure 20a) for the hydrogenated sample, suggests that the operation of the hydrogenated samples is quiet subtle with at least two competing processes driving their operation. The nature of these processes was still under investigation at the time of writing.

Chapter 5: Conclusions

III-V dilute nitrides offer potential as the additional layer in next generation multi-junction solar cells. GaInNAs is considered a good candidate since it has the potential to be lattice matched to current GaAs systems, while absorbing at 1 eV. However, the material quality of GaInNAs has been a concern. Although RTA is used to improve the material quality, by reducing point defects and catalyzing N-As substitution, the formation of stable N-N clusters and alloy fluctuations remains significant. Previously, hydrogenation of GaInNAs, and the complete passivation of substitutional nitrogen have been reported. Contrary to previous reports, in this project, it has been shown that selective hydrogen passivation can be achieved, with lower energy defects related to nitrogen clusters, and impurities passivated controllably using a UV-activated hydrogenation process. The selective passivation was observed in both GaInNAs bulk and solar cell samples optically using PL measurements, and in device characteristics using J-V and EQE measurements, including temperature dependent measurements. In temperature dependent PL measurements, clear improvements in optical quality and the removal of localized centers and defect-related states were observed upon hydrogenation. J-V and EQE measurements also confirmed that hydrogenation could improve the performance of passivated devices with respect to reference – as grown - solar cell devices.

In conclusion, this project – hydrogenation of dilute nitride materials for application to multi-junction solar cells – demonstrated the benefit of hydrogenation for GaInNAs material, providing a potential route to make these materials a *stronger* candidate for the fourth layer of next generation multi-junction solar cells.

References

[1] J. Nelson, *The Physics of Solar Cells*. London: Imperial College Press, 2003, p. 363.

[2] E. Becquerel, "Mèmoire sur les effets èlectriques produits sous l'influence des rayons solaires," *Comptes Rendus*, vol. 9, pp. 561–567, 1839.

[3] APS, "April 25, 1954: Bell Labs Demonstrates the First Practical Silicon Solar Cell," *APS News This Month in Physics History*, 2009. [Online]. Available: http://www.aps.org/publications/apsnews/200904/physicshistory.cfm.

[4] C. H. Henry, "Limiting efficiencies of ideal single and multiple energy gap terrestrial solar cells," *J. Appl. Phys.*, vol. 51, no. 8, pp. 4494–4500, 1980.

[5] C. Honsberg and S. Bowden, "PV Education.org." [Online]. Available: http://www.pveducation.org/. [Accessed: 20-Oct-2014].

[6] Y. P. Varshni, "Temperature dependence of the energy gap in semiconductors," *Physica*, vol. 34, no. 1, pp. 149–154, Jan. 1967.

[7] R. Ohl, "Light Sensitive Electric Device; Light-sensitive Electric Device Including Silicon," 240252; 2443542, 1941.

[8] M. a. Green, "The path to 25% silicon solar cell efficiency: History of silicon cell evolution," *Prog. Photovoltaics Res. Appl.*, vol. 17, no. 3, pp. 183–189, May 2009.

[9] W. Shockley and H. J. Queisser, "Detailed Balance Limit of Efficiency of p-n Junction Solar Cells," *J. Appl. Phys.*, vol. 32, no. 3, p. 510, 1961.

[10] L. C. Hirst and N. J. Ekins-daukes, "Fundamental losses in solar cells," in *Progress in Photovoltaics: Research and Applications*, vol. 19, no. August 2010, 2011, pp. 286–293.

[11] H. Cotal, C. Fetzer, J. Boisvert, G. Kinsey, R. King, P. Hebert, H. Yoon, and N. Karam, "III–V multijunction solar cells for concentrating photovoltaics," *Energy & Environmental Science*, vol. 2, no. 2. p. 174, 2009.

[12] B. Sciana, I. Zborowska-lindert, D. Radziewicz, D. Pucicki, and M. Panek, "Tunnel Junction Technology for Multijunction Solar Cell Applications," vol. 3, pp. 243–246, 2012.

[13] S. M. Bedair, M. F. Lamorte, and J. R. Hauser, "A two-junction cascade solar-cell structure," *Appl. Phys. Lett.*, vol. 34, no. 1, pp. 38–39, 1979.

[14] G. F. Virshup, B.-C. Chung, and J. G. Werthen, "23.9% monolithic multijunction solar cell," *Conf. Rec. Twent. IEEE Photovolt. Spec. Conf.*, 1988.

[15] J. F. Geisz and D. J. Friedman, "III N V semiconductors for solar photovoltaic applications," *Semiconductor Science and Technology*, vol. 17, no. 8. pp. 769–777, 2002.

[16] P. J. Klar, "Recent developmetns in metastable dilut-N III-V semiconductors," *Prog. Solid State Chem.*, vol. 31, pp. 301–349, 2003.

[17] M. Weyers, M. Sato, and H. Ando, "Red shift of photoluminescence and absorption in dilute GaAsN alloy layers," *Japanese J. Appl. Physics, Part 2 Lett.*, vol. 31, no. 7 A, 1992.

[18] D. J. Wolford, J. A. Bradley, K. Fry, and J. Thompson, "The Nitrogen Isoelectronic Trap in GaAs," in *Proceedings of the 17th International Conference on the Physics of Semiconductors*, J. D. Chadi and W. A. Harrison, Eds. New York: Springer New York, 1985, pp. 627–630.

[19] X. Liu, M.-E. Pistol, L. Samuelson, S. Schwetlick, and W. Seifert, "Nitrogen pair luminescence in GaAs," *Appl. Phys. Lett.*, vol. 56, no. 15, p. 1451, 1990.

[20] S. R. Kurtz, A. A. Allerman, E. D. : G. J. M. Jones, and J. J. Banas, "InGaAs Solar Cells with 1.0eV band gap. lattice matched to GaAs," *Appl. Phys. Lett.*, vol. 74, pp. 729–731, 1999.

[21] M. Kondow, T. Kitatani, S. Nakatsuka, M. C. Larson, K. Nakahara, Y. Yazawa, M. Okai, and K. Uomi, "GaInNAs: A novel material for long-wavelength semiconductor lasers," *IEEE J. Sel. Top. Quantum Electron.*, vol. 3, no. 3, pp. 719–729, 1997.

[22] K. Volz, J. Koch, B. Kunert, and W. Stolz, "Doping behaviour of Si, Te, Zn and Mg in lattice-matched (GaIn)(NAs)/GaAs bulk films," *J. Cryst. Growth*, vol. 248, pp. 451–456, Feb. 2003.

[23] A. R. Denton and N. W. Ashcroft, "Vegard's Law," *Phys. Rev. A*, vol. 43, no. 6, pp. 3161–3164, 1991.

[24] K. Volz, W. Stolz, J. Teubert, P. J. Klar, W. Heimbrodt, F. Dimroth, C. Baur, and A. W. Bett, "Doping, Electrical Properties and Solar Cell Application of GaInNAs," in *Dilute III-V Nitride Semiconductors and Material Systems Materials Science*, A. Erol, Ed. Springer Berlin Heidelberg, 2008, pp. 369–404.

[25] S. R. Kurtz, a. a. Allerman, C. H. Seager, R. M. Sieg, and E. D. Jones, "Minority carrier diffusion, defects, and localization in InGaAsN with 2% nitrogen," *Appl. Phys. Lett.*, vol. 77, no. 3, p. 400, 2000.

[26] M. Fukuda, V. R. Whiteside, J. C. Keay, M. B. Johnson, M. Al Khalfioui, M. Leroux, K. Hossain, T. D. Golding, and I. R. Sellers, "Selective passivation of nitrogen clusters and impurities in photovoltaic GaInNAs solar cells," *Photovolt. Spec. Conf. (PVSC), 2014 IEEE 40th*, pp. 0669 – 0673.

[27] D. J. Friedman, J. F. Geisz, S. R. Kurtz, and J. M. Olson, "1-eV solar cells with GaInNAs active layer," *J. Cryst. Growth*, vol. 195, no. 1–4, pp. 409–415, Dec. 1998.

[28] A. Aho, V. Polojärvi, V.-M. Korpijärvi, J. Salmi, A. Tukiainen, P. Laukkanen, and M. Guina, "Composition dependent growth dynamics in molecular beam epitaxy of GaInNAs solar cells," *Sol. Energy Mater. Sol. Cells*, vol. 124, pp. 150–158, May 2014.

[29] J. Neugebauer and C. G. Van de Walle, "Electronic structure and phase stability of GaAs/sub 1-x/N/sub x/ alloys," *Phys. Rev. B (Condensed Matter)*, vol. 51, no. 16, pp. 10568–10571, 1995.

[30] D. Schlenker, T. Miyamoto, Z. Pan, F. Koyama, and K. Iga, "Miscibility gap calculation for Ga In N As including \ V V W \ W strain effects," vol. 196, pp. 67–70, 1999.

[31] I. Ho and G. B. Stringfellow, "Solubility of nitrogen in binary III–V systems," *J. Cryst. Growth*, vol. 178, no. 1–2, pp. 1–7, Jun. 1997.

[32] A. J. Ptak, D. J. Friedman, S. Kurtz, and R. C. Reedy, "Low-acceptor-concentration GaInNAs grown by molecular-beam epitaxy for high-current p-i-n solar cell applications," *J. Appl. Phys.*, vol. 98, no. 9, p. 094501, 2005.

[33] W. McGee, R. Williams, M. Ashwin, T. Jones, E. Clarke, J. Zhang, and S. Tomić, "Structure, morphology, and optical properties of GaxIn1−xN0.05As0.95 quantum wells:Influence of the growth mechanism," *Phys. Rev. B*, vol. 76, no. 8, p. 085309, Aug. 2007.

[34] B. A. Joyce, "Molecular beam epitaxy," *Rep. Prog. Phys.*, vol. 48, p. 1637–1697, 1985.

[35] M. Kaminska, Z. Liliental-Weber, E. R. Weber, T. George, J. B. Kortright, F. W. Smith, B.-Y. Tsaur, and R. A. Calawa, "Structural properties of As-rich GaAs grown by molecular beam epitaxy at low temperatures," *Appl. Phys. Lett.*, vol. 54, no. 19, p. 1881, 1989.

[36] X. Liu, a. Prasad, J. Nishio, E. R. Weber, Z. Liliental-Weber, and W. Walukiewicz, "Native point defects in low-temperature-grown GaAs," *Appl. Phys. Lett.*, vol. 67, no. 2, p. 279, 1995.

[37] A. Khan, S. R. Kurtz, S. Prasad, S. W. Johnston, and J. Gou, "Correlation of nitrogen related traps in InGaAsN with solar cell properties Correlation of nitrogen related traps in InGaAsN with solar cell properties," vol. 243509, 2007.

[38] A. J. Å. Ptak, R. France, C. Jiang, and M. J. Romero, "Improved performance of GaInNAs solar cells grown by molecular-beam epitaxy using increased growth rate instead of surfactants," vol. 311, pp. 1876–1880, 2009.

[39] E.-M. Pavelescu, J. Wagner, H.-P. Komsa, T. T. Rantala, M. Dumitrescu, and M. Pessa, "Nitrogen incorporation into GaInNAs lattice-matched to GaAs: The effects of growth temperature and thermal annealing," *J. Appl. Phys.*, vol. 98, no. 8, p. 083524, 2005.

[40] E. S. Tok, J. H. Neave, J. Zhang, B. a. Joyce, and T. S. Jones, "Arsenic incorporation kinetics in GaAs(001) homoepitaxy revisited," *Surf. Sci.*, vol. 374, no. 1–3, pp. 397–405, Mar. 1997.

[41] I. R. Sellers, W. S. Tan, K. Smith, S. Hooper, S. Day, and M. Kauer, "Wide depletion width of 1 eV GaInNAs solar cells by thermal annealing," *Appl. Phys. Lett.*, vol. 99, p. 151111, 2011.

[42] K. Volz, D. Lackner, I. Németh, B. Kunert, W. Stolz, C. Baur, F. Dimroth, and a. W. Bett, "Optimization of annealing conditions of (GaIn)(NAs) for solar cell applications," *J. Cryst. Growth*, vol. 310, no. 7–9, pp. 2222–2228, Apr. 2008.

50

[43] S. Kurtz, J. Webb, L. Gedvilas, D. Friedman, J. Geisz, J. Olson, R. King, D. Joslin, and N. Karam, "Structural changes during annealing of GaInAsN," *Appl. Phys. Lett.*, vol. 78, no. 6, p. 748, 2001.

[44] D. B. Jackrel, S. R. Bank, H. B. Yuen, M. a. Wistey, J. S. Harris, A. J. Ptak, S. W. Johnston, D. J. Friedman, and S. R. Kurtz, "Dilute nitride GaInNAs and GaInNAsSb solar cells by molecular beam epitaxy," *J. Appl. Phys.*, vol. 101, no. 11, p. 114916, 2007.

[45] A. Polimeni and M. Capizzi, "Role of hydrogen in dilute nitrides," in *Physics and applications of dilute nitrides*, Illustrate., I. Buyanova and W. Chen, Eds. New York: Taylor & Francis, 2004, pp. 161–195.

[46] E. Mol, Z. Arbeiten, H. Sr, and D. Temperaturabh, "Die Wirkung von Wasserstoff auf die Leitfähigkeit und Lumineszenz von Zinkoxydkristallen," vol. 488, no. 1953, 1954.

[47] A. Van Wieringen and N. Warmoltz, "On the permeation of hydrogen and helium in single crystal silicon and germanium at elevated temperatures," *Physica*, vol. 22, no. 6–12, pp. 849–865, 1956.

[48] M. Bissiri, G. Baldassarri Höger von Högersthal, a. Polimeni, V. Gaspari, F. Ranalli, M. Capizzi, a. Bonapasta, F. Jiang, M. Stavola, D. Gollub, M. Fischer, M. Reinhardt, and a. Forchel, "Hydrogen-induced passivation of nitrogen in GaAs1-yNy," *Phys. Rev. B*, vol. 65, no. 23, p. 235210, Jun. 2002.

[49] I. a. Buyanova, W. M. Chen, M. Izadifard, S. J. Pearton, C. Bihler, M. S. Brandt, Y. G. Hong, and C. W. Tu, "Hydrogen passivation of nitrogen in GaNAs and GaNP alloys: How many H atoms are required for each N atom?," *Appl. Phys. Lett.*, vol. 90, no. 2, p. 021920, 2007.

[50] A. Polimeni, G. Baldassarri H. V., H. Bissiri, M. Capizzi, M. Fischer, M. Reinhardt, and A. Forchel, "Effect of hydrogen on the electronic properties of InxGa1-xAs1-yNy/GaAs quantum wells," *Phys. Rev. B*, vol. 63, no. 20, p. 201304, Apr. 2001.

[51] A. Polimeni, G. H. Baldassarri, M. Capizzi, G. B. H. ger von H gersthal, M. Bissiri, A. Frova, M. Fischer, M. Reinhardt, and A. Forchel, "Role of hydrogen in III – N – V compound," *Semicond. Sci. Technol.*, vol. 17, no. 8, pp. 161–195, 2002.

[52] Y. Tsai, B. Barman, T. Scrace, G. Lindberg, M. Fukuda, V. R. Whiteside, J. C. Keay, M. B. Johnson, I. R. Sellers, M. A. Khalfioui, M. Leroux, B. A. Weinstein, and A. Petrou, "Probing the nature of carrier localization in GaInNAs epilayers by optical methods," *Appl. Phys. Lett.*, vol. 103, p. 012104, 2013.

[53] C. H. Seager, "Hydrogenation Methods," in *Hydrogen in Semiconductors: Hydrogen in Silicon Volume 34*, J. I. Pankove and N. M. Johnson, Eds. Boston: Academic Press, 1991, pp. 17–33.

[54] M. N. Johnson, C. Herring, and D. J. Chadi, "Interstitial Hydrogen and Neutralization of Shallow Donor Impurities in Single-Crystalline Silicon," *Phys. Rev. Lett.*, vol. 56, p. 769, 1986.

Appendix A: List of Related Publications and Presentations

Publications

Y. Tsai, B. Barman, T. Scrace, G. Lindberg, M. Fukuda, V. R. Whiteside, J. C. Keay, M. B. Johnson, I. R. Sellers, M. A. Khalfioui, M. Leroux, B. A. Weinstein, and A. Petrou, "Probing the nature of carrier localization in GaInNAs epilayers by optical methods," *Appl. Phys. Lett.*, vol. 103, p. 012104, 2013.

M. Fukuda, V. R. Whiteside, J. C. Keay, M. B. Johnson, M. Al Khalfioui, M. Leroux, K. Hossain, T. D. Golding, and I. R. Sellers, "Selective passivation of nitrogen clusters and impurities in photovoltaic GaInNAs solar cells," *Photovolt. Spec. Conf. (PVSC), 2014 IEEE 40th* , pp. 0669 – 0673.

Y. Tsai, B. Barman, T. Scrace, M. Fukuda, V. R. Whiteside, I. R. Sellers, M. Leroux, M. A. Khalfioui, and A. Petrou, "Photoluminescence study of Me-acceptors in GaInNAs epilayers," *Appl. Phys. Lett.* – under review 14-Nov-2014.

M. Fukuda, V. R. Whiteside, J. C. Keay, M. Al Khalfioui, M. Leroux, K. Hossain, T. D. Golding, and I. R. Sellers, "Enhanced GaInNAs solar cell perfromance via hydrogen passivation of nitrogen-related defects," *Appl. Phys. Lett.* – in preparation Nov-2014.

Presentations

M. Fukuda, V. R. Whiteside, J. C. Keay, M. B. Johnson, M. Al Khalfioui, M. Leroux, K. Hossain, T. D. Golding, and I. R. Sellers, "Selective Passivation of GaInNAs Solar Cells by Hydrogenation," *APS March Meeting 2014.* Vol.59, No.1. Sessions M22: Hydrogen Storage, Transportation & Novel PV.

Appendix B: Symbols

Constants

c speed of light

h Planck's constant

k Boltzmann's constant

λ wavelength of incident photon

q charge on the electron

Symbols and Acronyms Used in the Thesis

η efficiency

AM   air mass

b_s incident spectral photon flux density

E   energy

E_g band gap energy

FF   fill factor

Isc   short circuit current

J_m current density at maximum power point

Jsc   short circuit current density

P_s incident light power density

QE   quantum efficiency

IQE   internal quantum efficiency

EQE   external quantum efficiency

R   resistance

T   temperature

V_{oc} open circuit voltage

V_m voltage at maximum power point

This volume is the property of the University of Oklahoma, but the literary rights of the author are a separate property and must be respected. Passages must not be copied or closely paraphrased without the previous written consent of the author. If the reader obtains any assistance from this volume, he or she must give proper credit in his own work.

I grant the University of Oklahoma Libraries permission to make a copy of my thesis/dissertation upon the request of individuals or libraries. This permission is granted with the understanding that a copy will be provided for research purposes only, and that requestors will be informed of these restrictions.

NAME _____

DATE _____

A library which borrows this thesis/dissertation for use by its patrons is expected to secure the signature of each user.

This thesis/dissertation by MIWA FUKUDA has been used by the following persons, whose signatures attest their acceptance of the above restrictions.

NAME AND ADDRESS   DATE

_____